PCCP

ROYAL SOCIETY OF CHEMISTRY

PAPER

View Article Online
View Journal | View Issue

Cite this: *Phys. Chem. Chem. Phys.*, 2024, **26**, 3920

A structural study on a specific Li-ion ordered complex in dimethyl carbonate-based dual-cation electrolytes†

Yu Chikaoka, *[ab] Tomoya Tashiro,[c] Saki Sawayama,[c] Ayana Kobayashi,[a] Ayuna Matsumoto,[a] Etsuro Iwama, [ab] Katsuhiko Naoi *[ab] and Kenta Fujii *[c]

Received 14th November 2023,
Accepted 26th December 2023

DOI: 10.1039/d3cp05526d

rsc.li/pccp

Dimethyl carbonate (DMC) is a linear carbonate solvent commonly used as an electrolyte for electric double-layer capacitors (EDLCs) and Li-ion batteries. However, there are serious problems with the use of DMC as an electrolyte solvent: (1) low ionic conductivity when using Li salts (*e.g.* $LiBF_4$) and (2) liquid–liquid phase separation when using spiro-type quaternary ammonium salts (*e.g.* $SBPBF_4$). Dual-cation electrolytes, *i.e.*, bi-salt ($SBPBF_4$ and $LiBF_4$) in DMC, are promising candidates to avoid the phase separation issue and to enhance the total and Li^+ conductivities. Herein, we reported a specific Li-ion structure in DMC-based dual-cation electrolytes by combining high-energy X-ray total scattering (HEXTS) and all-atom molecular dynamics (MD) simulations. Quantitative radial distribution function analysis based on experimental and simulation results revealed that the phase-separated $SBPBF_4$/DMC (*i.e.*, the bottom phase of 1 M $SBPBF_4$/DMC) forms long-range ion ordering based on the structured SBP^+–BF_4^- ion pairs. When adding $LiBF_4$ salt into $SBPBF_4$/DMC (*i.e.*, dual-cation electrolyte), the ordered SBP^+–BF_4^- structure disappeared owing to the formation of Li-ion solvation complexes. We found that in the dual-cation electrolyte Li ions form multiple Li^+–Li^+ ordered complexes in spite of relatively low Li-salt concentration (1 M), being a promising Li^+-conducting medium with reduced Li salt usage and low viscosity.

Introduction

Electrical energy storage systems (EESS) with good safety and high power are critical for the efficient use of energy and management of energy supply. In addition, EESS are key technologies towards a sustainable society. Electric double-layer capacitors (EDLCs), lithium-ion batteries, and hybrid capacitors are among the energy storage devices under development for commonly used EESS.[1–9] These EESS use several aprotic solvents as electrolytes to achieve the desired electrochemical performance. Some of the most employed solvents include cyclic carbonates (propylene carbonate – PC and ethylene carbonate – EC), linear carbonates (dimethyl carbonate – DMC, ethyl methyl carbonate – EMC, and diethyl carbonate – DEC), and others (acetonitrile – AN and sulfolane – SL).[10–15] Among these solvents, linear carbonates such as DMC have a low viscosity (0.59 cP at 20 °C)[10] and a low polarizability, resulting in a lower charge-transfer resistance of the Li^+ insertion/extraction reaction (*ca.* 40 kJ mol^{-1}) compared to another aprotic solvent based system (*ca.* 50–60 kJ mol^{-1}).[16] Thus, using a linear carbonate as a main solvent is beneficial for high power applications. However, the combination of DMC solvent and chemically stable BF_4-based salts presents some critical issues: (i) using $LiBF_4$ salts results in significantly low ionic conductivity (0.5 mS cm^{-1}) compared to $LiBF_4$/PC systems (3 mS cm^{-1}).[17,18] In addition, (ii) using quaternary ammonium salts (*i.e.*, 1,1′-spiropyrrolidinium (or 5-azoniaspiro[4.4]nonane tetrafluoroborate – $SBPBF_4$)) or ionic liquids (*i.e.* 1-ethyl-3-methylimidazolium tetrafluoroborate – $EMIBF_4$) enhances the ionic conductivity (up to 15–20 mS cm^{-1}); however, undesired liquid–liquid phase separation is a common problem in this case. For instance, 1 M $SBPBF_4$/DMC yields phase separation into nearly pure DMC as the upper phase and 2 M $SBPBF_4$/DMC as the bottom phase.[17]

Regarding the phase separation behavior, Wang *et al.* reported that mixing strong Lewis acid cations (*e.g.* Li^+) might minimize this issue in a phase-separated co-solvent of water

[a] *Department of Applied Chemistry, Tokyo University of Agriculture and Technology, 2-24-16 Naka-cho, Koganei, Tokyo 184-8558, Japan. E-mail: chika@go.tuat.ac.jp, k-naoi@cc.tuat.ac.jp*
[b] *Global Innovation Research Organization, Tokyo University of Agriculture & Technology, 2-24-16 Naka-cho, Koganei, Tokyo, 184-8588, Japan*
[c] *Graduate School of Sciences and Technology for Innovation, Yamaguchi University, 2-16-1 Tokiwadai, Ube, Yamaguchi 755-8611, Japan. E-mail: k-fujii@yamaguchi-u.ac.jp*

† Electronic supplementary information (ESI) available. See DOI: https://doi.org/10.1039/d3cp05526d

and DMC.[19] Recently, we proposed that introducing a dual-cation system comprising Li salt ($LiBF_4$) and additional electrolytic solvents ($SBPBF_4$) can generate a stable DMC-based electrolyte solution; that is, mixing 1 M $LiBF_4$ into 1 M $SBPBF_4$/DMC (that is phase-separated at 1 : 1 vol%) produces a single-phase solution with moderate–high ionic conductivity (5.9 mS cm^{-1}) relative to a single Li salt system (1 M $LiBF_4$/DMC).[17] Moreover, the DMC-based dual-cation system showed a high Li^+ conductivity of 1.4 mS cm^{-1} (defined as the product of total ionic conductivity and the Li^+ transport number) compared to PC-based dual-cation electrolytes (0.9 mS cm^{-1}), although both electrolytes have similar overall ionic conductivities. Owing to these improvements, the DMC-based dual-cation system achieved high-rate performance (88% capacity retention at 50 mA cm^{-2}) in Li^+-based energy storage systems.[17] However, to the best of our knowledge, the origin of the phase separation behavior in $SBPBF_4$/DMC and the high Li^+ conduction in DMC-based dual-cation electrolytes is still unknown. Several studies indicated that the ionic hydrophobicity may cause such specific liquid–liquid phase separation,[20] even though the detailed mechanism and solution structure are yet to be unraveled. Considering that DMC is a promising solvent for energy storage systems in high-power applications, the understanding of the origin of the phase separation behavior and ways to increase the ionic conduction is pivotal.

Herein, we thus investigated the solution structure of DMC-based dual-cation electrolytes using quaternary ammonium or imidazolium salts and $LiBF_4$ *via* the combined high-energy X-ray total scattering (HEXTS) with all-atom molecular dynamics (MD) simulations. Based on the radial distribution function analysis, we propose a specific Li-ion ordered structure, which triggers high Li^+ conduction, in the DMC-based dual-cation system. Our findings may provide a new perspective on the use of the DMC solvent and specific salts, such as Li and quaternary ammonium salts, as well as ionic liquids and other Mg^{2+}- and Ca^{2+}-based salts.

Experimental

Materials

$LiBF_4$ (Kishida Chemicals), $SBPBF_4$ (Carlit Holdings), and $EMIBF_4$ (Kishida Chemicals) were used as electrolytic salts. DMC and PC (Kishida Chemicals) were used as solvents. All the chemicals were used as received without any post treatment or purification process. The salts and solvents were mixed in a volumetric flask in an Ar-filled glovebox (Unico, dew point: −70 °C) to obtain the single-cation ($LiBF_4$/DMC, $SBPBF_4$/DMC, and $EMIBF_4$/DMC) and dual-cation ($SBPBF_4$/DMC and $EMIBF_4$/DMC with $LiBF_4$) electrolytes.

Measurements

The ionic conductivity was measured using an ionic conductivity meter (Mettler Toledo, S230 and InLab 710) at 298 K. High-energy X-ray total scattering (HEXTS) measurements were carried out using high-energy X-ray diffraction apparatus (BL04B2 beamline at SPring-8, JASRI, Japan) at room temperature with monochromatized 61.6 keV X-rays by a Si (200) monochromator.[21] The methodology for performing HEXTS measurements has been detailed in our previous reports.[22–24] The X-ray scattering intensities were corrected for factors (absorption, polarization, and incoherent scatterings) to obtain coherent scattering intensities, $[I_{coh}(q)]$. The experimental X-ray structure factor $[S^{exp}(q)]$ per stoichiometric volume and radial distribution function $[G^{exp}(r)]$ were obtained according to eqn (1) and (2):

$$S^{exp}(q) = \frac{\frac{I_{coh}(q)}{N} - \sum n_i f_i(q)^2}{\left[\sum n_i f_i(q)\right]^2} + 1 \quad (1)$$

$$G^{exp}(r) - 1 = \frac{1}{2\pi^2 r \rho_0}\int_0^{q_{max}} q[S^{exp}(q) - 1]\sin(qr)\frac{\sin\left(\frac{q\pi}{q_{max}}\right)}{\frac{q\pi}{q_{max}}}dq \quad (2)$$

where n_i is the number of atom i, $f_i(q)$ is the atomic scattering factor of atom i, ρ_0 is the density of atom i, N is the number of atoms in stoichiometric volume, and q_{max} is the maximum value of q (herein, 25 $Å^{-1}$). All-atom molecular dynamics (MD) simulations were conducted under the isothermal–isobaric (NPT) ensemble at 298 K and 1 atm in a cubic cell. The simulation time was 10 ns for all the systems examined to be in the equilibrium state. The methodology for the MD simulations has been outlined in our previous studies.[25–27] The composition of ions and solvents in the cubic box, and the resulting density (g cm^{-3}) at the equilibrium state are listed in Table S1 (ESI†). The force field parameters and partial charges used herein are described in detail in the ESI† (Fig. S1). Using the trajectories from the MD simulations, we determined the X-ray-weighted $S(q)$ and $G(r)$ functions [$S^{MD}(q)$ and $G^{MD}(r)$, respectively] to compare with the experimental functions; the details are described in the ESI.† Density functional theory (DFT) calculations were performed using Gaussian 09 software.[28] The optimized geometries of the Li-ion complexes, *i.e.*, $[Li(BF_4)_n(DMC)_m]^{1-n}$, were obtained *via* the calculation at the B3LYP/6-311** level, followed by normal frequency analysis. The binding energy (DE_{bind}) for the $Li(BF_4)_n(DMC)_m$ complex was calculated as the self-consistent field (SCF) energy difference between the complex and its individual components (Li^+, BF_4^-, and DMC) according to the following relation: $DE_{bind} = E_{SCF}(complex) - mE_{SCF}(BF_4) - nE_{SCF}(DMC)$, which was corrected by the basis set superposition error using the counterpoise method.[29]

Results and discussion

Phase behavior of DMC-based electrolytes

Fig. 1 shows the phase behavior of the single-cation ($LiBF_4$/DMC, $SBPBF_4$/DMC, $EMIBF_4$/DMC) and the dual-cation ($LiBF_4$/DMC with $SBPBF_4$ or $EMIBF_4$) electrolytes. In general, the DMC-based electrolytes with LiX salts (X: Cl, BF_4, PF_6, *etc.*) yield a stable

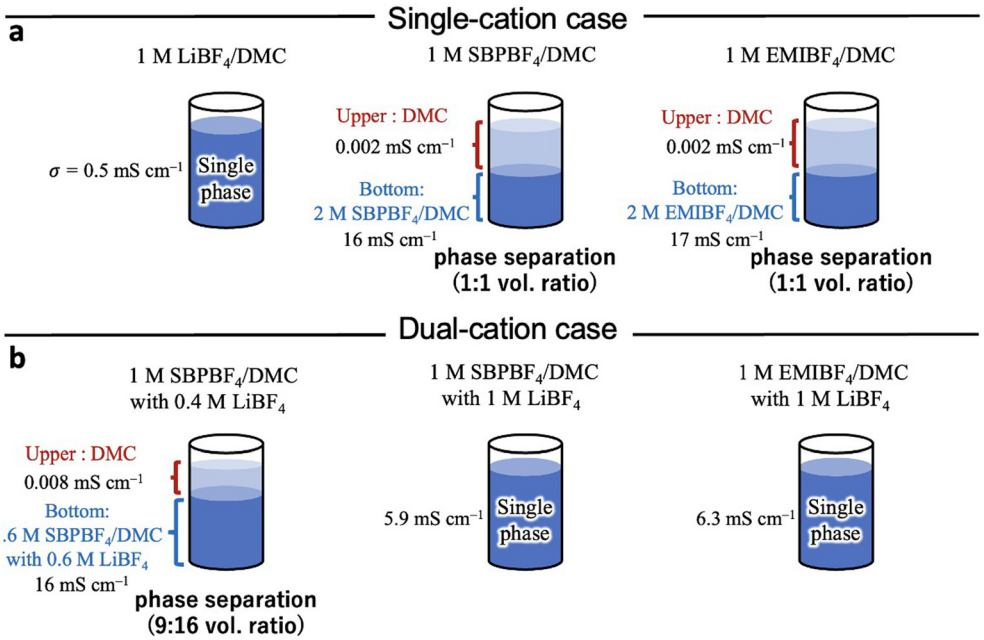

Fig. 1 Liquid phase behaviors and ionic conductivities (σ) of (a) the single-cation (1 M $LiBF_4$/DMC, 1 M $SBPBF_4$/DMC, 1 M $EMIBF_4$/DMC) and (b) the dual-cation (1 M $SBPBF_4$/DMC with 0.4 or 1 M $LiBF_4$, 1 M $EMIBF_4$/DMC with 1 M $LiBF_4$) electrolytes. Note that 1 M $SBPBF_4$ and 1 M $SBPBF_4$/DMC with 0.4 M $LiBF_4$ showed phase separation at 1 : 1 and 9 : 16 volume ratios, respectively. Detailed physicochemical parameters (ionic conductivity, viscosity, density, and concentration) were described in our previous report.[17]

single-phase solution as shown in Fig. 1a (left);[17,30] however, when using the quaternary ammonium salt ($SBPBF_4$) or imidazolium-based ionic liquid ($EMIBF_4$) as an alternative to Li salt, phase separation into upper and bottom phases occurred (Fig. 1a, center and right). In 1 M $SBPBF_4$/DMC and 1 M $EMIBF_4$/DMC, the upper phase was a nearly pure DMC solvent and thus exhibits an extremely low ionic conductivity (0.002–0.008 mS cm^{-1}), whereas the bottom phase was a salt-rich solution (*ca.* 2 M) that exhibits high ionic conductivity (σ = 16–17 mS cm^{-1}). This phase separation was particularly stable, as it settles to a partitioned state even after shaking the mixture. The resulting solutions have different densities in each phase (upper: 1.066 g cm^{-3}, bottom: 1.155 g cm^{-3}, in 1 M $SBPBF_4$/DMC) according to our previous work.[17] We found that 1 M $SBPBF_4$/DMC turns to a single-phase solution when adding $LiBF_4$ salt to the phase-separated system as shown in Fig. 1b. For example, the addition of 0.4 M $LiBF_4$ salt yielded a 9 : 16 vol% phase-separated solution (Fig. 1b, left): nearly pure DMC (upper phase, σ = 0.008 mS cm^{-1}) and 1 M $SBPBF_4$/DMC with 0.6 M of $LiBF_4$ (bottom phase, σ = 16 mS cm^{-1}). Further increasing $LiBF_4$ concentration up to 1 M made it a complete single-phase solution (Fig. 1b, center), *i.e.*, 1 M $SBPBF_4$/DMC containing 1 M of $LiBF_4$: σ = 5.9 mS cm^{-1}. A similar behavior was observed in the 1 M $EMIBF_4$/DMC with 1 M $LiBF_4$ system (Fig. 1b, right). The mixture of $LiBF_4$ and $SBPBF_4$ or $EMIBF_4$ in DMC exhibited high ionic conductivity (σ = 5.9–6.3 mS cm^{-1}), which was 10 times higher than that in the single Li salt solution (1 M $LiBF_4$/DMC: 0.5 mS cm^{-1}). In addition, compared to the conventional PC-based dual-cation system (1 M $SBPBF_4$/PC with 1 M $LiBF_4$), the DMC-based system offers a higher Li^+ transference number (t_{Li^+}, PC: 0.17, DMC: 0.23) and Li^+ conductivity (PC: 0.9 mS cm^{-1}, DMC: 1.4 mS cm^{-1}), even though both electrolytes without $SBPBF_4$ have similar ionic conductivity (*ca.* 6 mS cm^{-1}).[17] To obtain the detailed structures of ions in the DMC-based electrolytes (particularly the Li-ion solvation structure), we conducted a combined HEXTS with MD simulations.

Ion solvation structure in DMC-based electrolytes

Fig. 2 shows the X-ray structure factor $S(q)$ and its Fourier transform $G(r)$ as an r^2-weighted difference form ($r^2[G(r) - 1]$) obtained from HEXTS measurements and MD simulations for 1 M $SBPBF_4$/DMC solution with $LiBF_4$ salt (c_{Li} = 1 M). It is clear that in both $S(q)$ and $G(r)$ the simulated results (shown with solid red lines in Fig. 2) represent the HEXTS experimental values (open black circles). This strongly suggested that the force field parameters used in the current MD simulations are reasonable for describing the solution structure at the molecular level. Additional HEXTS and MD simulation results (1 M $LiBF_4$/DMC, 2 M $SBPBF_4$/DMC, and the bottom phase of 1 M $SBPBF_4$/DMC with 0.4 M $LiBF_4$) are provided in the ESI† (Fig. S2–S4). To obtain more insights into the solution structure, we divided total $G^{MD}(r)$ values into the respective contributions of cation–cation (SBP^+–SBP^+; $r^2[G^{MD}{}_{+,+}(r) - 1]$), anion–anion ($BF_4^-$–$BF_4^-$; $r^2[G^{MD}{}_{-,-}(r) - 1]$), and cation–anion ($SBP^+$–$BF_4^-$; $r^2[G^{MD}{}_{+,-}(r) - 1]$) interactions, which are shown in Fig. 3. Here, note that we performed the MD simulations for the 1 M $SBPBF_4$/DMC system as a model system, which is a

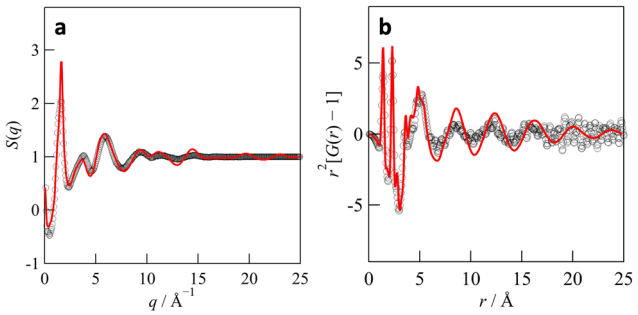

Fig. 2 (a) X-ray structure factor $S(q)$ and (b) radial distribution function in the difference form, $r^2[G(r) - 1]$, obtained from the HEXTS measurements (open black circles) and the MD simulations (solid red lines) for 1 M $SBPBF_4$/DMC with 1 M $LiBF_4$.

phase-separated solution (nearly pure DMC and 2 M $SBPBF_4$/DMC phases) in actual solution, to gain fundamental knowledge of the solvated SBP cations. In all systems, we observed a sharp peak around 5 Å in the $r^2[G^{MD}_{+,-}(r) - 1]$ function, corresponding to nearest-neighbor cation–anion interactions. This indicates that the SBP cations are electrostatically interacted with BF_4 anions to form ion pairs in DMC-based solutions, irrespective of $SBPBF_4$ salt concentration. In the long r-range (>5 Å), the 2 M $SBPBF_4$/DMC system showed several subsequent peaks for cation–anion correlations at ~11 Å, ~17 Å, and ~22 Å (Fig. 3b, top); however, only the second neighbor peak (~11 Å) was found in the 1 M $SBPBF_4$/DMC system (Fig. 3a, top). This result suggests that structuredness in solutions based on the SBP^+–BF_4^- ion pairs depends on the salt concentration, *i.e.*, concentrated $SBPBF_4$ salt in DMC-based solution produces a highly ionic ordered structure, like ionic liquids,[31,32] which is discussed in detail in the ESI† (long-range ordering in the $EMIBF_4$ ionic liquid; Fig. S5). We note that in the dual-cation case (1 M $SBPBF_4$/DMC with 1 M $LiBF_4$; Fig. 3c) the long-range ion–ion ordering disappeared by adding $LiBF_4$ salt. This result implies that the structured SBP^+–BF_4^- ion-pairs are ruptured owing to the formation of Li-ion solvation complexes, which is discussed in a later section. We expected that this ordered structure in $SBPBF_4$/DMC solution is related to the poor dissolution capability of $SBPBF_4$ salts, in other words the poor solvation power of the DMC solvent molecule, originating from the bulkiness and low polarization of the SBP cation and the low dielectric constant of DMC (3.1).[10] Indeed, the aforementioned dissolution process including phase separation does not occur in other linear carbonates (EMC and DEC) and cyclic carbonates (PC and EC) with high dielectric constants (60–90).[10,20,33,34]

Fig. 4 shows the atom–atom pair correlation functions, $g^{MD}_{X-Y}(r)$, for the O atoms (DMC) and F (BF_4^-) atoms around the Li ions in the DMC-based dual-cation systems, 1 M $SBPBF_4$/DMC with $LiBF_4$ (c_{Li} = 0.4 and 1 M), together with the single-cation solution, 1 M $LiBF_4$/DMC. In all electrolytes, nearest neighbor interactions for Li–DMC (Li–O) and Li–BF_4 (Li–B) appeared at 1.9 and 3.0 Å, respectively, which originated from the first solvation sphere of Li ions. The average coordination numbers $N(r)$ were calculated by integrating the corresponding $g^{MD}_{X-Y}(r)$ values up to a given r: ~2.1 Å and ~3.6 Å for Li–DMC and Li–BF_4 systems, respectively. In 1 M $LiBF_4$/DMC (Fig. 4a), the $N(r)$ values are 3.0 and 1.0 for Li–DMC and Li–BF_4 interactions, respectively, suggesting that the Li ions are coordinated with three DMC molecules and one BF_4 anion to form the charge-neutral Li-ion complex $[Li(BF_4)_1(DMC)_3]$ (Fig. 4d). When $LiBF_4$ coexisted with $SBPBF_4$ in the dual-cation electrolytes

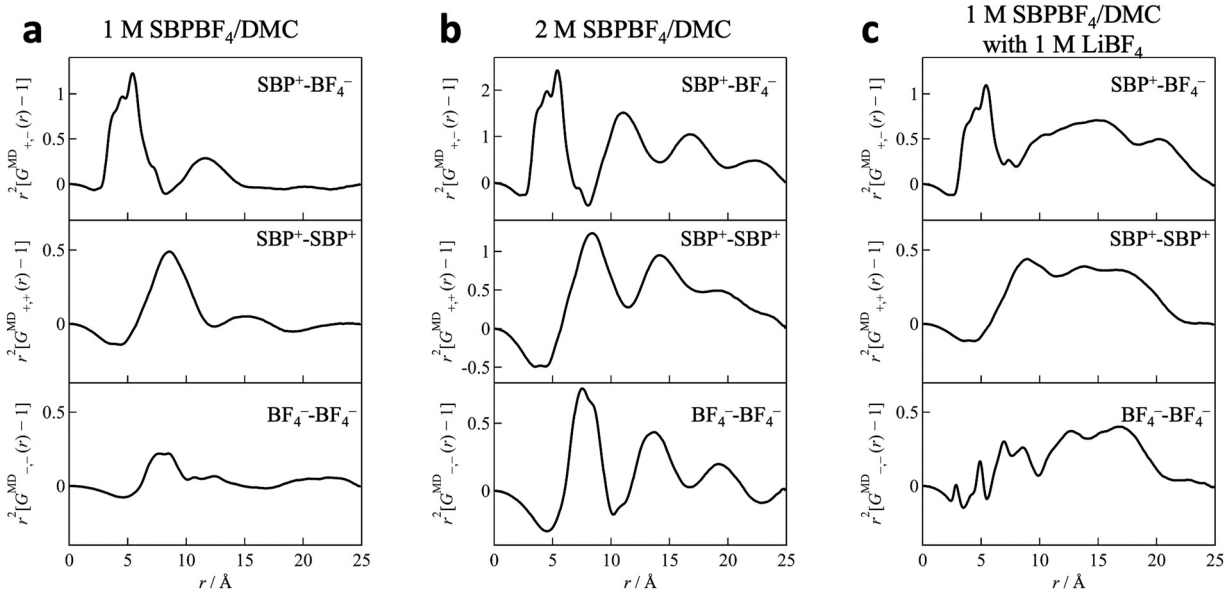

Fig. 3 Partial distribution functions for cation–cation (SBP^+–SBP^+; $r^2[G^{MD}_{+,+}(r) - 1]$), anion–anion (BF_4^-–BF_4^-; $r^2[G^{MD}_{-,-}(r) - 1]$), and cation–anion (SBP^+–BF_4^-; $r^2[G^{MD}_{+,-}(r) - 1]$) correlations in (a) 1 M $SBPBF_4$/DMC, (b) 2 M $SBPBF_4$/DMC, and (c) 1 M $SBPBF_4$/DMC with 1 M $LiBF_4$ solutions. Note that the single-phase solution of (a) 1 M $SBPBF_4$/DMC can be obtained only in the current model simulation because its actual solution shows a phase separation into neat DMC and 2 M $SBPBF_4$/DMC at 1 : 1 vol%.

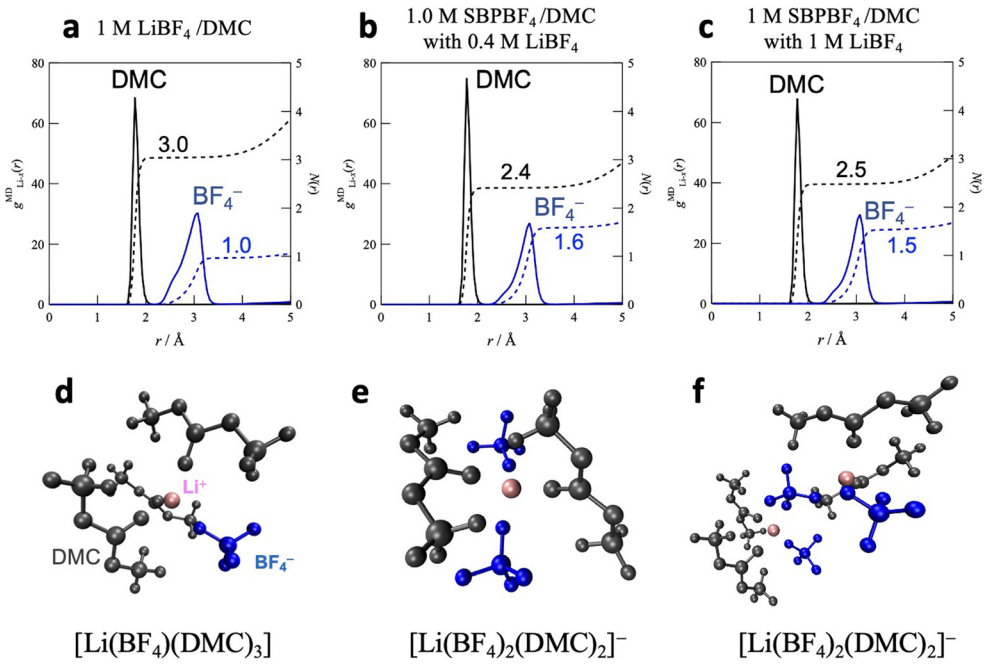

Fig. 4 Atom–atom pair correlation function, $g^{MD}_{X-Y}(r)$, for the O atoms (DMC) and the F atoms (BF_4^-) around Li ions in (a) 1 M $LiBF_4$/DMC, (b) the bottom phase of 1.0 M $SBPBF_4$/DMC with 0.4 M $LiBF_4$, and (c) 1 M $SBPBF_4$/DMC with 1 M $LiBF_4$. (d)–(f) Typical snapshots of Li-ion complexes confirmed in the simulation box for their solutions.

(Fig. 4b and c), the coordination number of DMC decreased to 2.4–2.5, while that of the BF_4 anion increased to 1.5–1.6, irrespective of the Li salt concentration, indicating the formation of the charged $[Li(BF_4)_2(DMC)_2]^-$ complex as an average structure (Fig. 4e and f). This result is consistent with the Li-ion coordination structure determined based on quantitative analysis of Raman spectra as reported in our previous work,[17] that is, $[Li(BF_4)_1(DMC)_3]$ in 1 M $LiBF_4$/DMC and $[Li(BF_4)_2(DMC)_2]^-$ in 1 M $SBPBF_4$/DMC with 0.4–1 M $LiBF_4$. We thus concluded that the $SBPBF_4$ salt triggers a change in the Li ion complexes from the neutral to the negatively charged state in DMC-based solutions. This may lead to a higher ionic conductivity in the dual-cation electrolyte (σ = 5.9 mS cm^{-1}) compared with the single-cation $LiBF_4$/DMC (σ = 0.5 mS cm^{-1}), as mentioned above (Fig. 1).

Here, we focus on the coordination manner of BF_4 anions around the central Li ion in Li-ion complexes. The BF_4 anion can act as both monodentate and bidentate ligands. If the BF_4 anion coordinates with a Li ion *via* two F atoms (bidentate ligand), the Li ions need to form a $[Li(BF_4)_1(solvent)_2]$ complex; this is because the total coordination number of Li ions is approximately 4 as is well known. In the current HEXTS and MD studies, however, this is not the case, *i.e.*, the BF_4 anions bind as a monodentate ligand to form $[Li(mono\text{-}BF_4)_1(DMC)_3]$ (single-cation) and $[Li(mono\text{-}BF_4)_2(DMC)_2]^-$ (dual-cation) complexes. This result was reasonable from the viewpoint of stabilization energy in the Li-ion complex formation by DFT calculations (Fig. 5). We calculated the binding energy (DE_{bind}) for the possible complex $[Li(mono\text{-}BF_4)_1(DMC)_3]$ and then compared it with that for the model bidentate-type complex

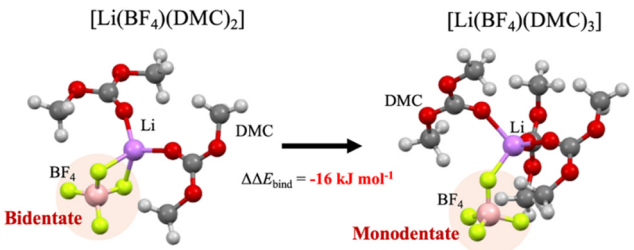

Fig. 5 Optimized geometries of possible $[Li(BF_4)(DMC)_2]$ (bidentate) and $[Li(BF_4)(DMC)_3]$ (monodentate) complexes by DFT calculations and their energy difference ($\Delta\Delta E_{bind}$) calculated from their binding energies ΔE_{bind}.

$[Li(bi\text{-}BF_4)_1(DMC)_2]$. The energy difference from the monodentate-type to the bidentate-type complex was estimated to be −16 kJ mol^{-1}. This indicates that the monodentate-type complex is more stable than the bidentate one, which agrees with the MD results in this work.

Fig. 6 shows the Li^+–Li^+ correlations, $g^{MD}_{Li-Li}(r)$, in single- and dual-cation electrolytes. In the single-cation electrolyte (1 M $LiBF_4$/DMC; Fig. 6a), a major broad peak was found at 8.9 Å, followed by around ∼17 Å, though there was a small peak at 5.2 Å. This 8.9 Å-peak originated from the correlation between mononuclear Li-ion solvation clusters (herein the $[Li(BF_4)_1(DMC)_3]$ complex),[35] and thus we concluded no closest Li^+–Li^+ correlation over the long-*r* range. On the other hand, the dual-cation electrolyte (Fig. 6b) exhibits strong closest Li^+–Li^+ peaks at 4–5 Å (overlapping 4.4 Å with 5.3 Å) and the subsequent clear peaks around 9 and 13 Å. This strongly suggests that a multiple ordered (or polymeric) Li-ion complex was

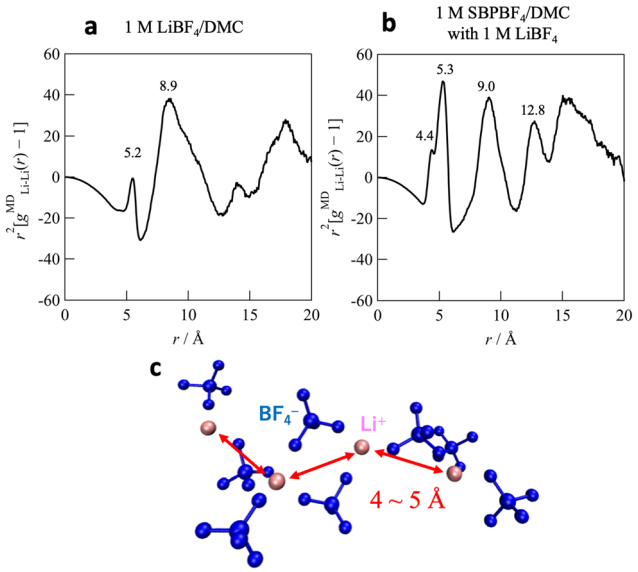

Fig. 6 Atom–atom pair correlation functions between Li ions [$g^{MD}_{Li-Li}(r)$] for (a) 1 M $LiBF_4$/DMC and (b) 1 M $SBPBF_4$/DMC with $LiBF_4$ (c_{Li} = 1 M). (c) Typical MD snapshots of Li-ion complexes found in 1 M $SBPBF_4$/DMC with $LiBF_4$.

formed in the dual-cation electrolyte, which is similar to the specific Li-ion ordered structure formed in highly concentrated electrolytes for Li-ion batteries, *i.e.*, organic and/or ionic liquid-based electrolytes with an extremely high concentration of Li salt.[35–38] Fig. 6c displays a typical snapshot obtained from the MD simulations for the dual-cation electrolyte; a Li-ion ordering linked *via* BF_4 anions was clearly evident. Such an ordering formation might help to show high Li^+ conductivity in dual-cation electrolyte systems, *e.g.*, Li-ion hopping conduction, as reported in highly concentrated electrolytes.[36,39–41] Indeed, DMC-based dual-cation electrolytes can achieve higher Li^+ conductivity ($\sim$1.5 mS cm^{-1}) than single-cation (0.2 mS cm^{-1}) or ordinary cyclic carbonate systems (PC-based dual-cation electrolytes, *ca.* 0.9 mS cm^{-1}).[17] We point out that, compared to the highly concentrated electrolyte (>3 M Li salt), our developed DMC-based dual-cation system allows the long-range Li^+–Li^+ ordered structure and high Li^+ conduction at a relatively low Li^+ concentration (*ca.* 1 M Li salt). Therefore, the DMC-based dual-cation system is a promising electrolyte with high Li^+ conductivity while presenting reduced Li salt concentration and low viscosity for optimum processability. Controlling the solution structure by incorporating several types of ions into the DMC solvent can be an effective strategy for achieving high power not only for Li^+-based electrolytes, but also for electrolytes with relatively high solvation energy such as Mg^{2+}- and Ca^{2+}-based systems.

Conclusions

We performed structural studies based on combined HEXTS experiments with MD simulations to demonstrate the unique solution structure in DMC-based dual-cation electrolytes. The radial distribution function $G(r)$ obtained from both HEXTS and MD results suggested an ion ordered structure based on SBP^+–BF_4^- ion pairs in the phase-separated 2 M $SBPBF_4$/DMC; in contrast, there was no ion ordering in 1 M $LiBF_4$/DMC solution. The ion ordered structure in $SBPBF_4$/DMC disappeared by adding $LiBF_4$ salt to form Li-ion solvation complexes alternatively, resulting in a single-phase solution, *i.e.*, dual-cation electrolyte. In dual-cation electrolyte (1 M $SBPBF_4$/DMC with 1 M $LiBF_4$), Li ions aggregate *via* BF_4 anions to form multiple Li-ion ordered complexes despite low Li salt concentration, and the structural feature was similar to those reported in highly concentrated Li-ion battery electrolytes using an organic solvent and Li salt (>3 M). We thus propose that DMC-based dual-cation electrolytes exhibit unique electrolytic properties arising from their specific solution structures to show great potential in the design of novel electrolytes with improved electrochemical properties, which are not limited to Li^+-based electrolytes.

Author contributions

The manuscript was written through contributions of all authors. All authors have given approval to the final version of the manuscript.

Conflicts of interest

The authors declare no conflicts of interest.

Acknowledgements

This study was supported by JSPS KAKENHI (grant no. JP19H00882 (KN), JP20H02823 (KF), 21K05241 (EI), 21K20554 (YC), 22K14759 (YC), and 23H02066 (KF)) and the Hitachi Metals and Materials Science Foundation (YC). The synchrotron radiation experiments were performed at SPring-8 with the approval of the Japan Synchrotron Radiation Research Institute (JASRI) (proposal no. 2021B1200 (KN), 2022A1174 (KN), 2023A1289 (KF), and 2023A1623 (SS)).

Notes and references

1 N. Omar, M. Daowd, O. Hegazy, M. Al Sakka, T. Coosemans, P. Van den Bossche and J. Van Mierlo, *Electrochim. Acta*, 2012, **86**, 305–315.
2 C. Schütter, S. Pohlmann and A. Balducci, *Adv. Energy Mater.*, 2019, **9**, 1900334.
3 S. Dong, N. Lv, Y. Wu, G. Zhu and X. Dong, *Adv. Funct. Mater.*, 2021, **31**, 2100455.
4 A. Muzaffar, M. B. Ahamed, K. Deshmukh and J. Thirumalai, *Renewable Sustainable Energy Rev.*, 2019, **101**, 123–145.
5 J. Sun, B. Luo and H. Li, *Adv. Energy Sustainability Res.*, 2022, **3**, 2100191.

6 X. Liu, Y. Sun, Y. Tong, X. Wang, J. Zheng, Y. Wu, H. Li, L. Niu and Y. Hou, *Nano Energy*, 2021, **86**, 106070.
7 A. Tomaszewska, Z. Chu, X. Feng, S. O'kane, X. Liu, J. Chen, C. Ji, E. Endler, R. Li and L. Liu, *ETransportation*, 2019, **1**, 100011.
8 A. Manthiram, *Nat. Commun.*, 2020, **11**, 1550.
9 H. Cheng, J. G. Shapter, Y. Li and G. Gao, *J. Energy Chem.*, 2021, **57**, 451–468.
10 K. Xu, *Chem. Rev.*, 2004, **104**, 4303–4418.
11 K. Chiba, T. Ueda and H. Yamamoto, *Electrochemistry*, 2007, **75**, 664–667.
12 Y.-B. He, B. Li, M. Liu, C. Zhang, W. Lv, C. Yang, J. Li, H. Du, B. Zhang and Q.-H. Yang, *Sci. Rep.*, 2012, **2**, 913.
13 E. Logan and J. Dahn, *Trends Chem.*, 2020, **2**, 354–366.
14 M. Yuan and K. Liu, *J. Energy Chem.*, 2020, **43**, 58–70.
15 J. Xu, J. Zhang, T. P. Pollard, Q. Li, S. Tan, S. Hou, H. Wan, F. Chen, H. He, E. Hu, K. Xu, X.-Q. Yang, O. Borodin and C. Wang, *Nature*, 2023, **614**, 694–700.
16 Y. Kondo, T. Abe and Y. Yamada, *ACS Appl. Mater. Interfaces*, 2022, **14**, 22706–22718.
17 Y. Chikaoka, R. Ochi, K. Fujii, T. Ariga, M. Sakurai, A. Matsumoto, T. Ueda, E. Iwama and K. Naoi, *J. Phys. Chem. C*, 2022, **126**, 14389–14398.
18 S. Hwang, D.-H. Kim, J. H. Shin, J. E. Jang, K. H. Ahn, C. Lee and H. Lee, *J. Phys. Chem. C*, 2018, **122**, 19438–19446.
19 F. Wang, O. Borodin, M. S. Ding, M. Gobet, J. Vatamanu, X. Fan, T. Gao, N. Eidson, Y. Liang and W. Sun, *Joule*, 2018, **2**, 927–937.
20 A. B. McEwen, S. F. McDevitt and V. R. Koch, *J. Electrochem. Soc.*, 1997, **144**, L84.
21 S. Kohara, K. Suzuya, Y. Kashihara, N. Matsumoto, N. Umesaki and I. Sakai, *Nucl. Instrum. Methods Phys. Res., Sect. A*, 2001, **467–468**, 1030–1033.
22 S. Sawayama, A. Morinaga, H. Mimura, M. Morita, Y. Katayama and K. Fujii, *ACS Appl. Mater. Interfaces*, 2021, **13**, 6201–6207.
23 K. Fujii, R. Kanzaki, T. Takamuku, Y. Kameda, S. Kohara, M. Kanakubo, M. Shibayama, S.-I. Ishiguro and Y. Umebayashi, *J. Chem. Phys.*, 2011, **135**, 244502.
24 K. Fujii, Y. Soejima, Y. Kyoshoin, S. Fukuda, R. Kanzaki, Y. Umebayashi, T. Yamaguchi, S. Ishiguro and T. Takamuku, *J. Phys. Chem. B*, 2008, **112**, 4329–4336.
25 K. Hirosawa, K. Fujii, K. Hashimoto and M. Shibayama, *Macromolecules*, 2017, **50**, 6509–6517.
26 M. Shibata, S. Sawayama, M. Osugi and K. Fujii, *J. Mol. Liq.*, 2022, **366**, 120255.
27 M. Sogawa, S. Sawayama, J. Han, C. Satou, K. Ohara, M. Matsugami, H. Mimura, M. Morita and K. Fujii, *J. Phys. Chem. C*, 2019, **123**, 8699–8708.
28 M. J. Frisch, G. W. Trucks, H. B. Schlegel, G. E. Scuseria, M. A. Robb, J. R. Cheeseman, G. Scalmani, V. Barone, B. Mennucci and G. A. Petersson, *Gaussian 09*, Gaussian, Inc., Wallingford CT, 2009.
29 M. Asada, T. Fujimori, K. Fujii, R. Kanzaki, Y. Umebayashi and S. Ishiguro, *J. Raman Spectrosc.*, 2007, **38**, 417–426.
30 H. Lee, S. Hwang, M. Kim, K. Kwak, J. Lee, Y.-K. Han and H. Lee, *J. Phys. Chem. Lett.*, 2020, **11**, 10382–10387.
31 Y. Umebayashi, H. Hamano, S. Seki, B. Minofar, K. Fujii, K. Hayamizu, S. Tsuzuki, Y. Kameda, S. Kohara and M. Watanabe, *J. Phys. Chem. B*, 2011, **115**, 12179–12191.
32 R. Kanzaki, T. Mitsugi, S. Fukuda, K. Fujii, M. Takeuchi, Y. Soejima, T. Takamuku, T. Yamaguchi, Y. Umebayashi and S.-I. Ishiguro, *J. Mol. Liq.*, 2009, **147**, 77–82.
33 K. Chiba, T. Ueda and H. Yamamoto, *Electrochemistry*, 2007, **75**, 668–671.
34 T. Sukizaki, S. Fukuda, T. Yamaguchi, K. Fujii, R. Kanzaki, K. Chiba, H. Yamamoto, Y. Umebayashi and S.-I. Ishiguro, *Electrochemistry*, 2007, **75**, 628–634.
35 K. Fujii, M. Matsugami, K. Ueno, K. Ohara, M. Sogawa, T. Utsunomiya and M. Morita, *J. Phys. Chem. C*, 2017, **121**, 22720–22726.
36 K. Dokko, D. Watanabe, Y. Ugata, M. L. Thomas, S. Tsuzuki, W. Shinoda, K. Hashimoto, K. Ueno, Y. Umebayashi and M. Watanabe, *J. Phys. Chem. B*, 2018, **122**, 10736–10745.
37 Y. Yamada, J. Wang, S. Ko, E. Watanabe and A. Yamada, *Nat. Energy*, 2019, **4**, 269–280.
38 K. Shigenobu, M. Shibata, K. Dokko, M. Watanabe, K. Fujii and K. Ueno, *Phys. Chem. Chem. Phys.*, 2021, **23**, 2622–2629.
39 S. Kondou, M. L. Thomas, T. Mandai, K. Ueno, K. Dokko and M. Watanabe, *Phys. Chem. Chem. Phys.*, 2019, **21**, 5097–5105.
40 Y. Ugata, M. L. Thomas, T. Mandai, K. Ueno, K. Dokko and M. Watanabe, *Phys. Chem. Chem. Phys.*, 2019, **21**, 9759–9768.
41 Y. Watanabe, Y. Ugata, K. Ueno, M. Watanabe and K. Dokko, *Phys. Chem. Chem. Phys.*, 2023, **25**, 3092–3099.

